Observation of Optical Vortices and J_0 Bessel-Like Beams in Quantum-Noise Parametric Amplification

Paolo Di Trapani,[1,*] Audrius Beržanskis,[2,†] Stefano Minardi,[1] Samantha Sapone,[1] and Walter Chinaglia[1]
[1]*INFM, University of Insubria, Institute of Mathematical, Physical and Chemical Sciences, via Lucini 3, 22100 Como, Italy*
[2]*Department of Physical and Medical Engineering, University of Applied Sciences, PF 100 314, 07703 Jena, Germany*
(Received 29 June 1998)

We show that optical vortices and J_0 Bessel-like beams can be generated via traveling-wave linear parametric amplification of the quantum noise, in the absence of external seeding or resonator feedback. The shot-to-shot fluctuations in the topological charge of the amplified signal are driven by the quantum-noise seed. [S0031-9007(98)07767-9]

PACS numbers: 42.65.Yj, 42.50.Lc

Optical fields with a ring-shaped angular spectrum, whose radial profile is close to the Bessel J_n functions, remarkably enrich the linear and nonlinear dynamics of light beams. The J_0 Bessel-like beam shows very low diffraction [1], and fulfills nontrivial phase-matching (PM) conditions in second-harmonic generation [2]. The higher-order J_n Bessel-like beams are optical vortices [3], with a screw dislocation [4] of quantized topological charge n. Such charge can exhibit a "bit"-like behavior under algebraic all-optical processing [5]. Moreover, vortices have angular momentum [6], whose conservation introduces new perspectives into the wave-particle analogy [7]. In the linear regime, vortices can be generated by filtering smooth-wave-front waves with passive optical elements (like phase plates [8], holograms [9], or speckle diffusors [10]); in propagation, they show steering and rotation in the absence of interaction [11]. In the nonlinear regime, on the other hand, vortex generation is assisted by multistability or self-organization phenomena [12,13], as observed, for example, in a photorefractive resonator [14]; the nonlinear propagation is enriched by the soliton regime, currently under major investigation [8,11,15–19].

The experiment described in this Letter demonstrates that highly coherent Bessel-like optical vortices ("OV," in the following) and J_0 Bessel-like beams can be generated in a traveling-wave optical parametric amplifier (OPA) of the vacuum-state fluctuations (the quantum noise). Quantum-noise OPA's are commonly not considered as suitable sources of diffraction-limited radiation, so much so that external seeding or spatial filtering in multipass configurations are routinely adopted in order to achieve this limit in OPA-based commercial light sources. In a recent work [20], however, we have demonstrated that spatial mode locking can take place in a linear OPA pumped by a narrow Gaussian beam, in the case of a Gaussian angular gain profile. This mode locking is governed by the competition between beam narrowing (in the near field, due to the preferential amplification of the signal at the beam center) and spectral narrowing (in the far field, due to the angular gain profile of the OPA). In fact, the beam narrowing increases the far-field correlation, whereas the spectral narrowing increases that in near field, until complete spatial coherence is achieved. Here we extend this approach to the case of an OPA with ring-shaped angular gain profile. The results show that the J_0 beam is the stationary (or fully mode-locked) state of such an OPA, which we obtained in the limit of very narrow Gaussian pump beam (with FWHM ≤ 35 μm). Slightly larger pumps lead to uncompleted mode-locking regime. In this case, clean OV beams occur with some probability too, the shot-to-shot fluctuation of the topological charge being controlled by the initial (quantum) noise seed.

The measurement consists in the monitoring of the near- and far-field energy distribution of the signal radiation generated via traveling-wave amplification of quantum noise in a 15 mm lithium triborate crystal (LBO). The amplification is obtained by using $\simeq 1$ ps, 527 nm pump pulses in Gaussian beam, in a regime of undepleted pump. The crystal is operated in noncritical phase matching, in order to avoid spatial walk-off and axial-symmetry breaking, and in type-II phase matching, in order to have temporal gain bandwidth sufficiently narrow to guarantee the temporal transform limit for the generated pulses. Note that in the absence of such a "quasimonochromatic" regime one should expect the excess bandwidth to cause a number of independent transverse structures within a single pulse, thus leading to an integrated effect at the CCD camera detector. The ring-shaped angular gain profile is obtained by filtering the temporal-frequency components of the output radiation by means of an 8.5 nm wide interferential filter, with transmission peaked at 960 nm. Because of the phase-matching constraints in the type-II LBO, this filtering causes the overall gain to peak at the outside surface of a nearly round cone, with the half-aperture of 28 mrad. Note that, because of the linearity of the amplification regime, the temporal signal frequencies not matched with the filter bandwidth do not contribute to the transverse structures seen by the detector.

Figure 1 shows the results of the single-shot measurements of the far- and near-field energy distributions of the amplified signal beam. They are obtained by splitting the

beam into two arms and sending them to the same camera, through suitable optics. Figures 1a and 1b refer to two typical different realizations, occurring with the same external parameters (i.e., pump intensity, $I_p = 30$ GW/cm^2, and FWHM pump-beam diameter, $d = 61$ μm). In both cases, the far field shows the expected smooth-ring profile. As to the near field, Fig. 1a shows a J_0 Bessel-like profile, embedded in a Gaussian envelope, which is consistent with the far field under the assumption of a constant phase over the ring. In Fig. 1b, on the other hand, the intensity distribution exhibits an evident dark spot in the center (just under the maximum of the pump intensity), the profile being close to that of a (Gaussian-embedded) Bessel J_n function with $n \neq 0$, i.e., the OV with charge n. The high spatial coherence follows from the clean near- and far-field profiles free from any substructure.

For the assigned pump-beam parameters, the probability of obtaining clean signal-beam profiles such as those in Figs. 1a and 1b is about 45% and 36%, respectively. In the remaining cases more complex structures, with a larger number of topological defects, are obtained. The probability of such noisy structures increases with the pump diameter, and the same filamentation or specklelike profiles as those shown in Ref. [21] were always obtained for d of several hundreds of μm. Moving towards the opposite limit of very narrow pump, on the other hand, we observed that all the topological defects tend to be removed, including the case of the single vortex. More precisely, we measured for the probability of the J_0-like beams, P_0, the following values: $P_0 = 20\%$, 45%, 60%, and 94%, for $d = 76$, 61, 50, and 35 μm, respectively, where $\simeq$130 shots for each diameter were considered. All the measurements were performed at $I_p \simeq 30$ GW/cm^2 except the last, in which double the intensity was used in order to prevent gain quenching due to large pump diffraction.

Figure 2 reports the results of the measurement of the topological charge of signal beams, such as those in Figs. 1a and 1b. They are obtained by sending the beam through a 4f imaging system [22], with a computer-generated forklike hologram [4,9] of a vortex placed in the Fourier plane between the two lenses. This filter behaves as a diffraction grating which adds a topological charge m to the mth-order diffracted beam. In the figure the effect of the hologram on the imaged near-field profiles for the $m = +1$ (left), $m = 0$ (center), and $m = -1$ (right) diffracted orders is evident. Figure 2a refers to the case of J_0 field. In fact, the $m = 0$ image, not affected by the hologram, has the profile of a J_0 beam, whereas both the $m = 1$ and $m = -1$ images show the dark central spots due to the vorticity added by the hologram. Figure 2b shows an OV with unitary charge: the $m = -1$ diffracted-beam image has a peak in the center, whereas the $m = 0$ and $m = 1$ beams exhibit a dark spot (OV of charges 1 and 2, respectively). Figure 2c presents an OV with opposite charge to that in Fig. 2b. We mention that the idler wave, at wavelength 1.17 μm, was not detected in our experiment due to the IR cutoff in the sensitivity of the silicon CCD camera. However, it is expected to have topological charge of opposite sign to the signal [5].

It is clear that the output radiation of our traveling-wave quantum-noise OPA shows well distinguishable macroscopic states, with quantized topological charge (and thus with angular momentum). The first question then concerns the circumstances which determine the "decision" of the system for a given output state. The hypothesis that the mechanism is driven by classical fluctuations in external control parameters (i.e., the boundary conditions imposed by the pump and the crystal) does not find any support

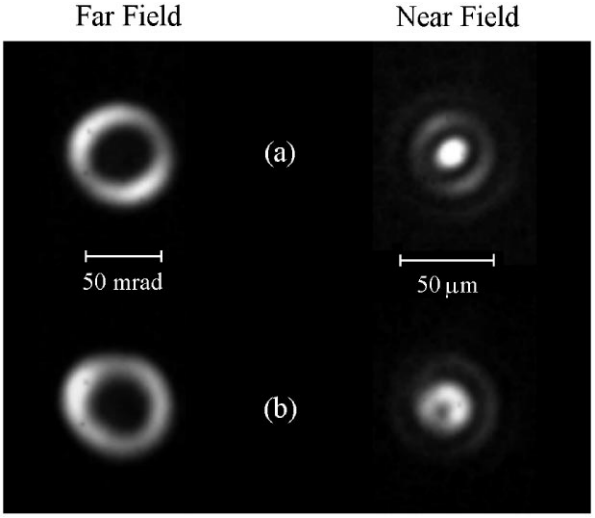

FIG. 1. Single-shot far-field and near-field profiles of the amplified signal beam. The two different realizations (a) and (b), obtained with the same pump parameters (pump intensity $I_p = 30$ GW/cm^2, FWHM $d = 61$ μm), refer to nonvortex and vortex fields, respectively.

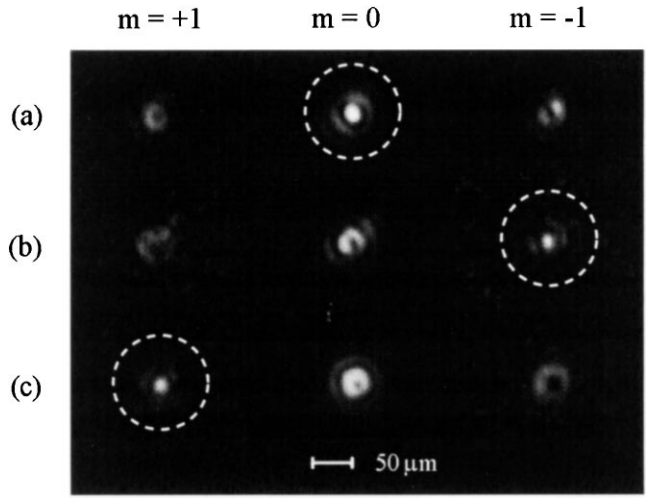

FIG. 2. Single-shot near-field profiles of the amplified signal beam at the 0th and $\pm$1st diffracted order of a grating fork hologram. (a) J_0; (b) J_1; (c) J_{-1} Bessel-like beams. Pump as in Fig. 1.

in our experiment. In fact, by deliberately changing the beam position in the crystal and the pump intensity (the last by 20%, i.e., more than twice the laser fluctuations) we did not observe any change in the output-charge statistics. Moreover, direct statistical measurements on the charge-sign probability show that the J_1 and J_{-1} beams appear with the same frequency, in contrast to what one expects in the case of vorticity induced by the crystal. The results suggest, therefore, that the single-shot output-charge value is essentially determined by the peculiarities of each realization of the input noise seed in the system, i.e., it has a purely quantum origin in our case. The quantum-noise influence on formation of vortices in optical systems was first investigated in [23], concerning the case of a laser source brought suddenly above threshold.

In order to better investigate the effects of the input-seed fluctuations, to characterize the dynamics of the structure formation and their stability under linear parametric amplification we performed a few numerical "experiments." In comparison with the real experiments, the numerical calculations have the advantage of controlling the input-seed conditions and allow the beam-profile evolution to be followed, inside an arbitrarily long crystal. To this end, we modeled our OPA with the standard three-wave coupled equations [24] in the monochromatic and undepleted-pump approximations, which we have shown to be consistent with our experimental regime.

Figure 3 presents two examples of the evolution of the near-field intensity (left), near-field phase (center), and the far-field intensity (right) of the signal field inside the crystal. The pump-beam parameters are as in Figs. 1 and 2. For the input seed we took a random-amplitude and random-phase (classical) field, with angular spectrum much broader than the OPA gain bandwidth. The results in Figs. 3a and 3b are obtained with two different realizations of the input seed, leading to a J_0 and to an $(n = 1)$ OV output, respectively, as is evident from the near-field intensity and phase profiles at $z = 15$ mm. The agreement with experiment is evident too. By independently changing the pump and the input-seed conditions we verified that, for a given seed, the topological charge of the output field is insensitive to small changes in the pump profile (of the same order as the fluctuations in the experiment) while, for a given pump, it critically depends on the input-seed profile. In contrast, the output-charge statistics appeared to be sensitive to large changes in the pump-beam diameter, and the observed disappearance of vortices in case of very narrow pump is well confirmed in the numerical experiments.

To verify whether this statistical trend is related to the stability of vortices under linear amplification we performed numerical calculations using a prepared vortex field, instead of noise, as the seeding signal. The results show that if the vortex is initially centered and has axial symmetry (with respect to the pump), then the amplification process does not change the topological charge of the field. Otherwise, it experiences a repulsion that can push it out of the signal beam before gain quenching due to pump diffraction occurs.

An example of such vortex expulsion is shown in the sequence in Fig. 4. One may note that while the near field transforms from a (Gaussian embedded) J_1 to a J_0 beam, in the far field the intensity of the ring first gets thinner on one side (Fig. 4b), later it brakes apart (i.e., the vortex leaves the inner part of the spectrum, Fig. 4c), and finally it closes back (the vortex is already outside, Fig. 4d). The transformation is evident in the phase profile too. This behavior should not be surprising. In fact, the spatial mode locking increases the far-field correlation in the radial direction, due to the radial gain modulation induced by the focused-pump profile [20]. Therefore, any defect which destroys the axial symmetry of the field experiences a sort of stress which tends to move it out of the gain region. The decreasing of the vortex probability with the pump-beam

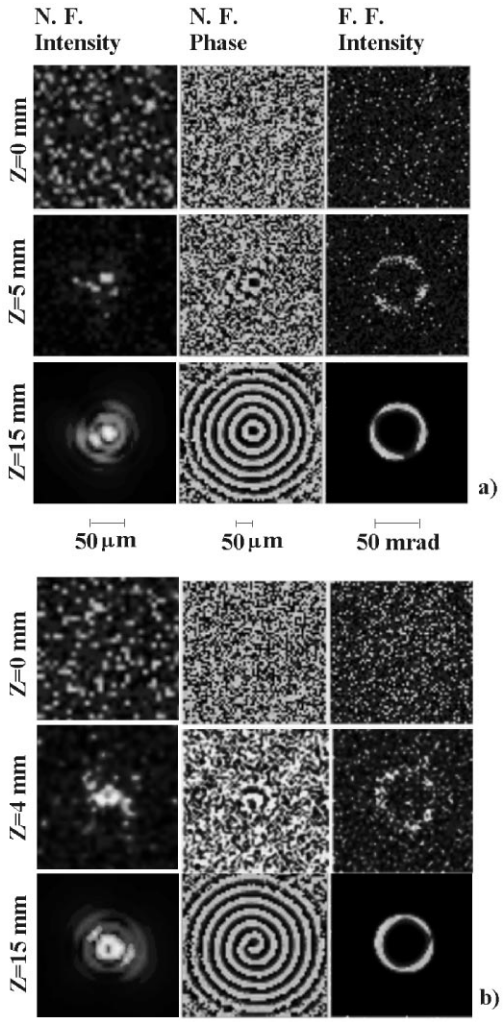

FIG. 3. Numerical results on the signal-field evolution inside the crystal in terms of the near-field intensity (left), phase (center), and of the far-field intensity (right) profiles. The two dynamics in (a) and (b), leading to nonvortex and to vortex fields, respectively, are obtained by changing the $z = 0$ noise signal. Pump parameters are taken as in Fig. 1.

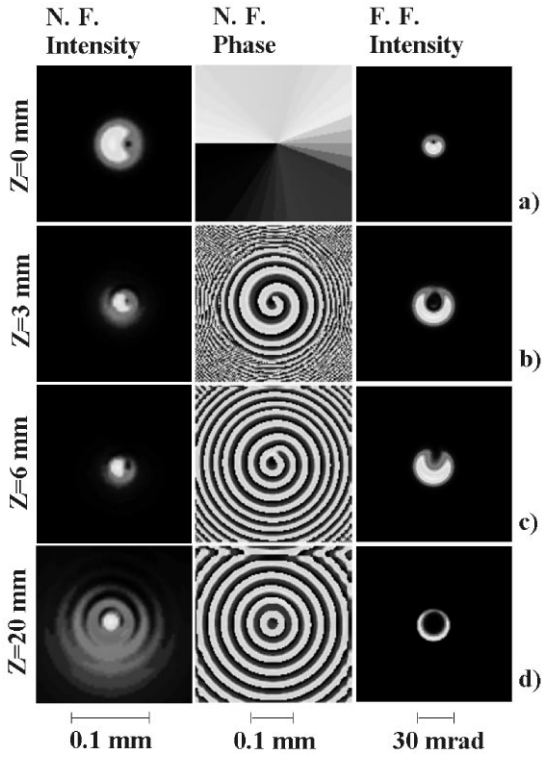

FIG. 4. Numerical results on vortex expulsion. Signal near-field intensity (left), phase (center), and the far-field intensity (right) profiles, at different z coordinate, in the crystal. Pump parameters: $I_p = 60$ GW/cm^2; $d = 35$ μm.

diameter can then be explained as a consequence of the enhancement in vortex repulsion with the gain gradient.

In conclusion, we have shown that Bessel-like vortices and J_0 Bessel-like beams can be generated in a traveling-wave, optical parametric amplifier with a ring-shaped gain spectrum, starting from the quantum noise. The experimental and numerical results indicate that the fluctuations in the initial quantum-noise control the macroscopic output-charge distribution. Statistic and dynamic investigations show that the J_0 Bessel-like beam is the only stable configuration of such an OPA, while the charged vortices tend to be expelled from the gain region, unless they are exactly centered with respect to the pump beam. Because of the finite length of the crystal, however, vortices can be generated with a large probability.

The authors acknowledge A. Matijošius, V. Smilgevičius, and A. Piskarskas for helpful discussions. The research has been partially supported by the MURST 9702268683-001 and CNR 97.00070.CT02 projects and by the CRUI-Vigoni program.

*Electronic address: DITRAPAN@FIS.UNICO.IT
†Permanent address: Vilnius University, Laser Research Center, Sauletekio Avenue 9, building 3, 2040 Vilnius, Lithuania.

[1] J. Durnin, J. J. Miceli, Jr., and J. H. Eberly, Phys. Rev. Lett. **58**, 1499 (1987).
[2] T. Wulle and S. Herminghaus, Phys. Rev. Lett. **70**, 1401 (1993).
[3] A. Vasara, J. Turunen, and A. T. Friberg, J. Opt. Soc. Am. A **6**, 1748 (1989).
[4] I. Basistiy, V. Bazhenov, M. Soskin, and M. Vasnetsov, Opt. Commun. **103**, 422 (1993).
[5] A. Beržanskis, A. Matijošius, A. Piskarskas, V. Smilgevičius, and A. Stabinis, Opt. Commun. **140**, 273 (1997).
[6] L. Allen, M. W. Beijersbergen, R. J. C. Spreeuw, and J. P. Woerdman, Phys. Rev. A **45**, 8185 (1992).
[7] W. J. Firth and D. V. Skryabin, Phys. Rev. Lett. **79**, 2450 (1997).
[8] G. A. Swartzlander, Jr. and C. T. Law, Phys. Rev. Lett. **69**, 2503 (1992).
[9] V. Y. Bazhenov, M. S. Soskin, and M. V. Vasnetsov, J. Mod. Opt. **39**, 985 (1992).
[10] N. B. Baranova, A. V. Mamaev, N. F. Pilipetsky, V. V. Shkunov, and B. Ya. Zeldovich, J. Opt. Soc. Am. **73**, 525 (1983).
[11] D. Rozas, C. T. Law, and G. A. Swartzlander, Jr., J. Opt. Soc. Am. B **14**, 3054 (1997).
[12] L. A. Lugiato, Phys. Rep. **219**, 293 (1992).
[13] C. O. Weiss, Phys. Rep. **219**, 311 (1992).
[14] F. T. Arecchi, G. Giacomelli, P. L. Ramazza, and S. Residori, Phys. Rev. Lett. **67**, 3749 (1991); F. T. Arecchi, S. Boccaletti, P. L. Ramazza, and S. Residori, Phys. Rev. Lett. **70**, 2277 (1993).
[15] G. Duree, M. Morin, G. Salamo, M. Segev, B. Crosignani, P. Di Porto, E. Sharp, and A. Yariv, Phys. Rev. Lett. **74**, 1978 (1995).
[16] B. Luther-Davies, R. Powles, and V. Tikhonenko, Opt. Lett. **19**, 1816 (1994).
[17] Z. Chen, M. Segev, D. W. Wilson, R. E. Muller, and P. D. Maker, Phys. Rev. Lett. **78**, 2948 (1997).
[18] K. Staliunas, Chaos Solitons Fractals **4**, 1783 (1994).
[19] A. V. Mamaev, M. Saffman, and A. A. Zozulya, Phys. Rev. Lett. **76**, 2262 (1996).
[20] P. Di Trapani, W. Chinaglia, and A. Andreoni, in *Proceedings of the EQEC '96 Conference* (IEEE, New York, 1996); P. D. Trapani, G. Valiulis, W. Chinaglia, and A. Andreoni, Phys. Rev. Lett. **80**, 265 (1998).
[21] A. Gatti, L. A. Lugiato, G. Oppo, R. Martin, P. D. Trapani, and A. Beržanskis, Opt. Express **1**, 21 (1997).
[22] See, for example, B. E. A. Saleh and M. C. Teich, *Fundamentals of Photonics* (Wiley, New York, 1991), pp. 136 and 148.
[23] P. Coullet, L. Gil, and F. Rocca, Opt. Commun. **73**, 403 (1989).
[24] W. E. Torruellas, Z. Wang, D. J. Hagan, E. W. VanStryland, G. I. Stegeman, L. Torner, and C. R. Menyuk, Phys. Rev. Lett. **74**, 5036 (1995).